Soluble Epoxide Hydrolase Deficiency Attenuates Neointima Formation in the Femoral Cuff Model of Hyperlipidemic Mice

Marc Revermann, Manuel Schloss, Eduardo Barbosa-Sicard, Anja Mieth, Stefan Liebner, Christophe Morisseau, Gerd Geisslinger, Ralph T. Schermuly, Ingrid Fleming, Bruce D. Hammock and Ralf P. Brandes

Arterioscler Thromb Vasc Biol 2010;30;909-914; originally published online Mar 11, 2010;
DOI: 10.1161/ATVBAHA.110.204099
Arteriosclerosis, Thrombosis, and Vascular Biology is published by the American Heart Association. 7272 Greenville Avenue, Dallas, TX 72514
 Print ISSN: 1079-5642. Online ISSN: 1524-4636

Soluble Epoxide Hydrolase Deficiency Attenuates Neointima Formation in the Femoral Cuff Model of Hyperlipidemic Mice

Marc Revermann, Manuel Schloss, Eduardo Barbosa-Sicard, Anja Mieth, Stefan Liebner, Christophe Morisseau, Gerd Geisslinger, Ralph T. Schermuly, Ingrid Fleming, Bruce D. Hammock, Ralf P. Brandes

Objective—Epoxyeicosatrienoic acids (EETs) have antiinflammatory effects and are required for normal endothelial function. The soluble epoxide hydrolase (sEH) metabolizes EETs to their less active diols. We hypothesized that knockout and inhibition of sEH prevents neointima formation in hyperlipidemic ApoE$^{-/-}$ mice.

Methods and Results—Inhibition of sEH by 12-(3-adamantan-1-yl-ureido) dodecanoic acid or knockout of the enzyme significantly increased plasma EET levels. sEH activity was detectable in femoral and carotid arteries. sEH knockout or inhibition resulted in a significant reduction of neointima formation in the femoral artery cuff model but not following carotid artery ligation. Although macrophage infiltration occurred abundantly at the site of cuff placement in both sEH$^{+/+}$ and sEH$^{-/-}$, the expression of proinflammatory genes was significantly reduced in femoral arteries from sEH$^{-/-}$ mice. Moreover, an in vivo 5-bromo-2′-deoxyuridine assay revealed that smooth muscle cell proliferation at the site of cuff placement was attenuated in sEH knockout and sEH inhibitor–treated animals.

Conclusion—These observations suggest that inhibition of sEH prevents vascular remodeling in an inflammatory model but not in a blood flow–dependent model of neointima formation. **(*Arterioscler Thromb Vasc Biol*. 2010;30:909-914.)**

Key Words: epoxyeicosatrienoic acids ■ lipid mediators ■ neointima ■ migration ■ smooth muscle cells

Neointima formation is an important clinical problem contributing to vaso-occlusive diseases, such as restenosis after coronary angioplasty or atherosclerosis. The process is complex and, at least in rodents, involves proliferation of smooth muscle cells (SMCs) in response to growth factors (such as platelet-derived growth factor), migration of SMCs into the subendothelial layer,[1] and recruitment of monocytes and transdifferentiation of circulating progenitor cells at the site of the lesion.[2] Many systemic and local factors modulate these events. Mechanical injury, inflammation, oxidative stress,[3] and hyperlipidemia promote neointima formation, whereas nitric oxide (NO), generated by either endothelial or inducible NO synthases, attenuates neointima formation.[4]

Several different models of neointima development can be studied in rodents. In almost every model, hyperlipidemia, induced by fat feeding or genetic deletion of the low-density lipoprotein receptor or apolipoproteins, is a prerequisite for neointima formation, which is then combined with a second stimulus.[5] Such a second stimulus is usually an alteration in blood flow and subsequent changes in local endothelial NO production, as it occurs in the carotid artery ligation model[6]; mechanical injury and endothelial denudation, as in the oversized balloon model; or vascular irritation induced by a foreign body, as in the femoral artery cuff model.[4] Although all of these interventions promote neointima formation, the degree of inflammation and the contribution of NO to the process vary considerably. In general, the femoral artery cuff model is considered more inflammatory than the carotid ligation model, the latter being dominated by NO withdrawal.

Nitric oxide, however, is not the only vasoprotective endothelial autacoid. Prostacyclin and epoxyeicosatrienoic acids (EETs) also contribute to the antiatherosclerotic properties of the endothelium. Indeed, EETs, which are derived from arachidonic acid by epoxygenation through cytochrome P450 monooxygenases, mediate endothelium-dependent vasodilation, promote angiogenesis, and have antiinflammatory properties.[7] The availability of EETs is limited primarily by the soluble epoxide hydrolase (sEH), which metabolizes EETs to their corresponding dihydroxyeicosatrienoic acids (DHETs). DHETs show equivalent or reduced biological

Received on: February 8, 2009; final version accepted on: February 9, 2010.

From Institut für Kardiovaskuläre Physiologie/ZAFES (M.R., M.S., A.M., R.P.B.) and Institut für Neuropathologie (S.L.), Fachbereich Medizin der Goethe-Universität, Frankfurt am Main, Germany; Institute for Vascular Signalling, Centre for Molecular Medicine (E.B.-S., I.F.) and Pharmazentrum Frankfurt/ZAFES, Institut für Klinische Pharmakologie (G.G.), Klinikum der Goethe-Universität Frankfurt am Main, Germany; Department of Entomology and University of California Davis Cancer Center, University of California, Davis, Calif (C.M., B.D.H.); Max-Planck-Institute for Heart and Lung Research, Bad Nauheim, Germany (R.T.S.).

Correspondence to Ralf P. Brandes, Institut für Kardiovaskuläre Physiologie, Fachbereich Medizin der Goethe-Universität, Theodor-Stern-Kai 7, D-60596 Frankfurt am Main, Germany. E-mail r.brandes@em.uni-frankfurt.de

Arterioscler Thromb Vasc Biol **is available at http://atvb.ahajournals.org** **DOI: 10.1161/ATVBAHA.110.204099**

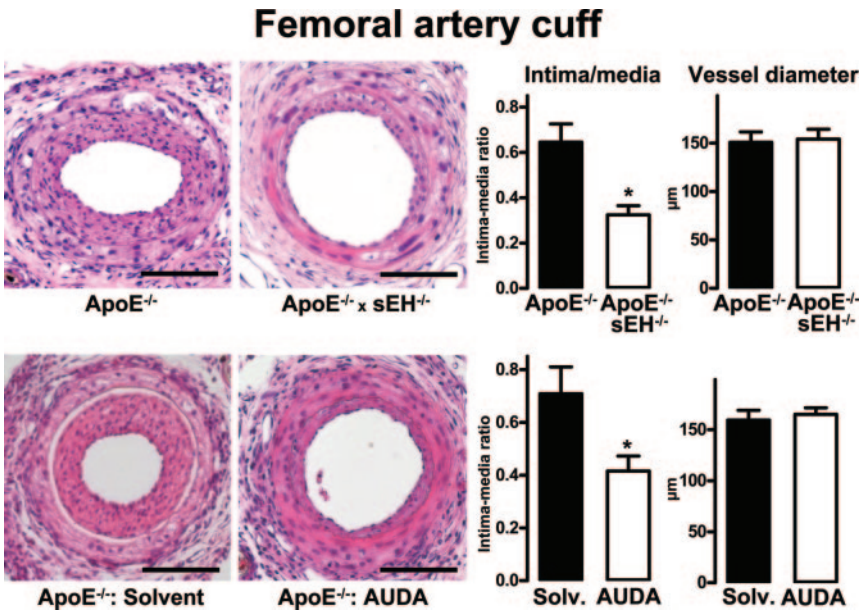

Figure 1. Neointima formation in femoral artery cuff model. Shown are representative sections and statistical analysis from ApoE$^{-/-}$ and ApoE$^{-/-}$×sEH$^{-/-}$ mice (top) and from ApoE$^{-/-}$ mice treated with solvent (Solv.) or AUDA (bottom) 2 weeks after cuff placement. Mean±SEM, n=9 to 13, *P<0.05. Scale bars=100 μm.

activity but are more hydrophilic and easily excreted.[8] sEH inhibitors lower blood pressure in different models of hypertension in rodents.[9,10] Moreover, these compounds attenuate the inflammatory response in models of endotoxemia and acute lung injury, as well as ischemic injury in stroke models in rats.

The role of vascular-derived EETs in the process of neointima formation is unknown and we hypothesized that increasing EET levels by inhibiting the sEH should attenuate neointima formation in hyperlipidemic ApoE$^{-/-}$ mice following placement of a femoral artery cuff and carotid artery ligation. The role of sEH was studied by generating sEH-ApoE double knockout mice and by the treatment with the sEH inhibitor 12-(3-adamantan-1-yl-ureido)-dodecanoic acid (AUDA).

Materials and Methods

An extended version of the Materials and Methods section can be found in the supplemental materials, available online at http://atvb.ahajournals.org.

Animal Models

The experiments were performed in accordance with the National Institutes of Health Guidelines on the Use of Laboratory Animals. Both the University Animal Care Committee and the Federal Authorities for Animal Research of the Regierungspräsidium Darmstadt (Hessen, Germany) approved the study protocol. C57/BL6-ApoE$^{-/-}$ breeding pairs (ApoE$^{-/-}$) were purchased from Charles River (Deisenhofen, Germany). C57/BL6-sEH$^{-/-}$ mice (F5, sEH$^{-/-}$) were kindly supplied by F. Gonzalez (National Institutes of Health, Bethesda, Md)[11] and crossed with ApoE$^{-/-}$ mice to obtain ApoE$^{-/-}$×sEH$^{-/-}$ animals. ApoE$^{-/-}$×sEH$^{-/-}$ were backcrossed more than 7 times to obtain ApoE$^{-/-}$×sEH$^{+/+}$. For the sake of readability, ApoE$^{-/-}$×sEH$^{+/+}$ are designated ApoE$^{-/-}$. The sEH inhibitor 12-(3-adamantan-1-yl-ureido)-dodecanoic acid (AUDA; final concentration, 100 mg/L)[12] was administered to the animals via drinking water. Neointima formation and accelerated atherosclerosis were induced by means of vascular injury through cuff placement around the femoral artery of mice or left common carotid artery ligation, as described previously.[4–6] Two weeks after cuff placement, respectively 4 weeks after carotid artery ligation, vessels were perfusion fixed, sectioned and analyzed by planimetry. In vivo cell proliferation was determined by 5-bromo-2′-deoxyuridine (BrdUrd) incorporation.

sEH and EET Detection

sEH protein was detected by Western blot analysis, whereas activity was determined by the conversion of 14,15-EET to 14,15-DHET. EETs and DHETs were measured by liquid chromatography-tandem mass spectrometry as described previously.[13]

Data and Statistical Analysis

All values are mean±SEM. Statistical analysis was performed using ANOVA, unpaired t test, and the Mann-Whitney test. A probability value of less than 0.05 was considered statistically significant.

Results

Loss of sEH Activity Attenuates Neointima Formation in the Femoral Artery Cuff Model

Two weeks after cuff placement, a marked neointima had developed in the femoral artery of ApoE$^{-/-}$ mice. In animals with genetic deletion or pharmacological inhibition of the sEH, the intima-media ratio was approximately 50% lower than in control animals (Figure 1). The outer vessel diameter as a parameter of inward or outward remodeling was, however, identical in all groups, demonstrating that a lack of sEH activity leads to attenuation of neointima formation in the femoral cuff model in ApoE$^{-/-}$ mice.

sEH Knockout Has No Effect on Neointima Formation Following Carotid Artery Ligation

In contrast to the data obtained in the femoral artery cuff model, genetic deletion of the sEH had no effect on neointima formation after carotid artery ligation. In ligated vessels, there was no difference in the intima-media ratio or in the constrictive remodeling between ApoE$^{-/-}$ and ApoE$^{-/-}$×sEH$^{-/-}$ mice (Figure 2). Given this negative result, the effect of sEH inhibition on neointima formation in this model was not tested in additional animal experiments.

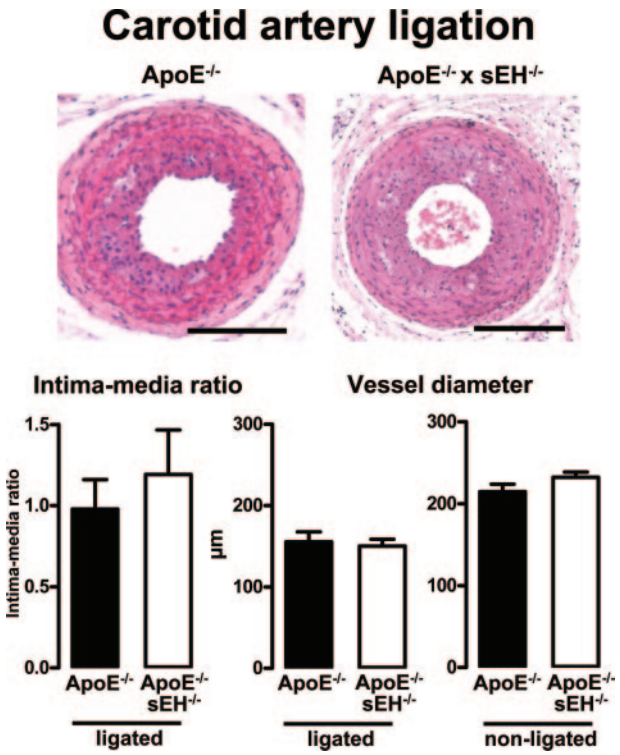

Figure 2. Neointima formation in carotid artery ligation model. Representative sections of the ligated left side (top) and statistical analysis (bottom) from ligated and nonligated arteries of ApoE$^{-/-}$ and ApoE$^{-/-}$×sEH$^{-/-}$ mice 4 weeks after surgery. Mean±SEM, n=8 to 9, *P*=not significant. Scale bars=100 μm.

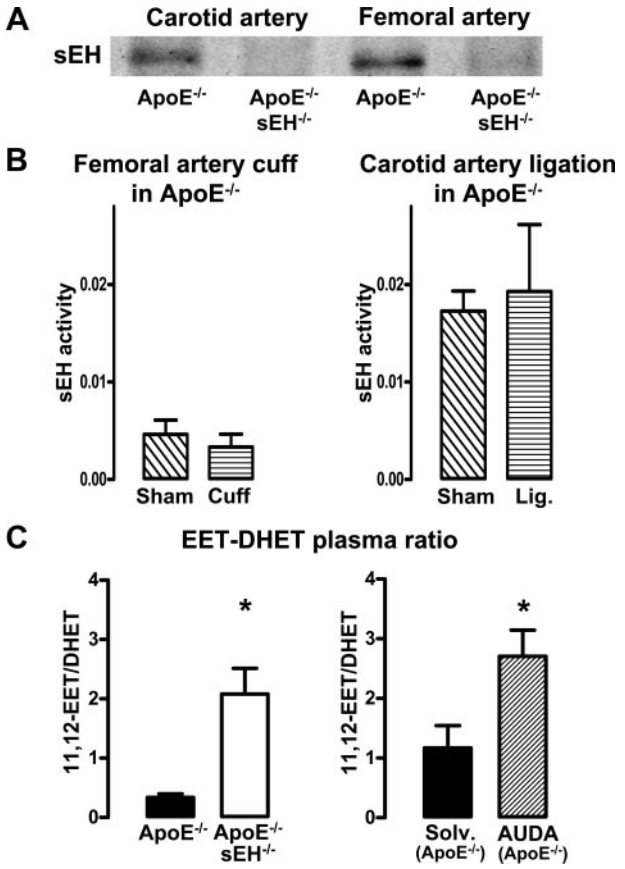

Figure 3. sEH and plasma EET concentrations. A, Representative Western blots for sEH in vascular extracts from ApoE$^{-/-}$ and ApoE$^{-/-}$×sEH$^{-/-}$ mice. B, sEH activity (units: ng of 14,15-DHET/μg of protein per minute) in vascular extracts from ApoE$^{-/-}$ mice subjected to sham operation, cuff placement, or carotid ligation. n=6, *P*=not significant. C, Plasma 11,12-EET to 11,12-DHET level ratio in ApoE$^{-/-}$ and ApoE$^{-/-}$×sEH$^{-/-}$ mice (left) and from ApoE$^{-/-}$ treated with solvent or AUDA (right). n=9 to 10, **P*<0.05.

sEH Is Expressed in the Vascular Wall of Murine Carotid and Femoral Arteries

sEH protein expression was detectable in femoral and carotid arteries of ApoE$^{-/-}$ but not in vessels of ApoE$^{-/-}$×sEH$^{-/-}$ mice (Figure 3A). Neither the femoral artery cuff nor the carotid artery ligation had a detectable effect on local sEH activity in ApoE$^{-/-}$ mice (Figure 3B). To demonstrate the impact of the sEH on plasma EET and DHET levels, the 4 EET and DHET regioisomers were determined (Supplemental Figure I). The ratios of 11,12-EET and 14,15-EET to their corresponding DHETs were significantly increased in ApoE$^{-/-}$×sEH$^{-/-}$ compared with ApoE$^{-/-}$ mice (Figure 3C and Supplemental Figure I). Accordingly, the sEH inhibitor AUDA increased the EET-DHET ratio in ApoE$^{-/-}$ mice (Figure 3C and Supplemental Figure I), as well. These data demonstrate that lack of sEH activity systematically increases the EET-DHET ratio, acutely as well as chronically, and that there is no local loss of sEH activity in both models that were used in this study.

Loss of sEH Activity Attenuates SMC Proliferation in the Femoral Artery Cuff Model

Neointima formation is, at least in part, a consequence of local proliferation and migration of SMCs. Indeed, immunohistology of operated femoral arteries revealed that the neointima in the cuff model consists mainly of smooth α-actin immunopositive cells, covered by an intact endothelium, as determined by platelet endothelial cell adhesion molecule 1 (PECAM-1) staining (Figure 4A). Macrophages or endothelial cells were almost absent in the neointima (Figure 4A). BrdUrd labeling showed a significant increase of SMC proliferation in response to femoral artery cuff placement and carotid artery ligation (Figure 4B through 4D). SMC proliferation in response to cuff placement was significantly attenuated in the femoral of ApoE$^{-/-}$ mice treated with the sEH inhibitors compared with solvent-treated animals (Figure 4B). Moreover, SMC proliferation was also significantly lower in the cuffed region of femoral arteries of ApoE$^{-/-}$×sEH$^{-/-}$ mice compared with ApoE$^{-/-}$ animals (Figure 4C). In line with the data on neointima formation, SMC proliferation in ligated carotid arteries was not affected by genetic deletion of the sEH (Figure 4D).

Genetic Deletion of the sEH Attenuates the Inflammatory Response in the Femoral Artery Cuff Model

As also obvious from the hematoxylin/eosin staining in Figures 1 and 2, the femoral artery cuff model, but not the carotid artery ligation model, presents with a marked adventitial inflammatory infiltrate (Figure 5A). As EETs have antiinflammatory effects, we concentrated on this aspect in

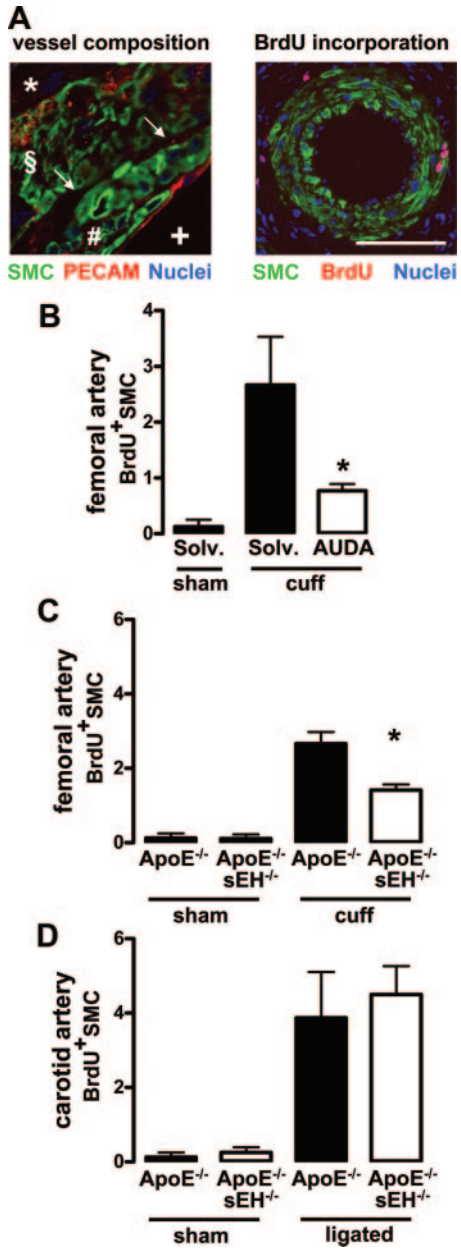

Figure 4. Vessel composition and SMC proliferation. A, Left, Representative section of the femoral artery of an ApoE$^{-/-}$ mouse after cuff placement. Platelet endothelial cell adhesion molecule 1 (PECAM-1) staining was used to identify endothelial cells. PECAM-1 staining also detected macrophages in the adventitia (+, vascular lumen; #, neointima; §, medial layer; *, perivascular area). Right, Representative image of BrdUrd incorporation (red) 14 days after operation in a femoral artery subjected to cuff placement. The color of the label corresponds to the stain indicated. Scale bar=100 μm. B through D, BrdUrd incorporation (mean BrdUrd immunopositive cells/orthogonal section) of AUDA-treated mice in comparison with solvent-treated animals 14 days after femoral artery cuff operation (n=4 to 7, *P<0.05) (B), of ApoE$^{-/-}$ and ApoE$^{-/-}$×sEH$^{-/-}$ 14 days after femoral artery cuff placement (n=6 to 7, *P<0.05) (C), and of ApoE$^{-/-}$ and ApoE$^{-/-}$×sEH$^{-/-}$ 28 days after carotid artery ligation (n=6, *P<0.05) (D).

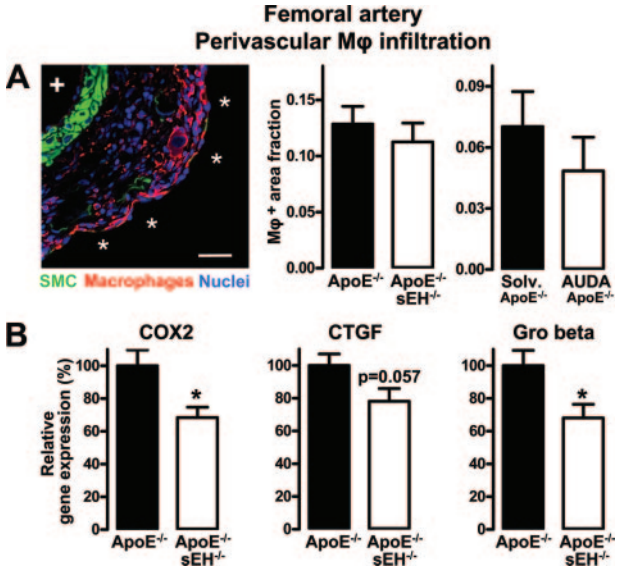

Figure 5. Perivascular inflammation. A, Left, Representative image of perivascular macrophage infiltration (F4/80 staining) of a femoral artery from an ApoE$^{-/-}$ mouse 14 days after cuff placement. The color of the label corresponds to the stain used. +, endovascular lumen; *, free space after cuff removal. Scale bar=40 μm. Right, F4/80 immunopositive perivascular area fraction in ApoE$^{-/-}$ and ApoE$^{-/-}$×sEH$^{-/-}$ mice 14 days after cuff placement. B, mRNA expression of the genes indicated as relative gene expression in the femoral arteries from ApoE$^{-/-}$ and ApoE$^{-/-}$×sEH$^{-/-}$ mice after cuff placement. n=7 to 8, *P<0.05.

the femoral artery model as a potential explanation for the antiproliferative effect of sEH inhibition. As determined by area coverage, the adventitial macrophage infiltrate was similar in ApoE$^{-/-}$ and ApoE$^{-/-}$×sEH$^{-/-}$ mice. Also, sEH inhibitor treatment had no significant effect on macrophage accumulation. In contrast, the sEH controlled the expression of some markers of inflammation: Gro-β and COX2 mRNA was significantly lower, and there was a trend toward a reduced connective tissue growth factor (CTGF) mRNA expression in sEH$^{-/-}$×ApoE$^{-/-}$ mice compared with ApoE$^{-/-}$ mice (Figure 5B). No difference between ApoE$^{-/-}$ and ApoE$^{-/-}$×sEH$^{-/-}$ was observed for expression of tumor necrosis factor-α (2.8±0.3 versus 2.5±0.5), Gro-α (7.0±1.2 versus 5.8±1.0), and MCP-1 (1.9±0.1 versus 1.7±0.2). Moreover, no differences in mRNA expression were observed between the groups in the carotid artery ligation model (data not shown).

Discussion

In the present study, we determined the role of the sEH in neointima formation in ApoE$^{-/-}$ mice. In the femoral artery cuff model, we observed that lack of sEH activity was associated with attenuated neointima formation, reduced SMC proliferation, and attenuated proinflammatory gene expression. In contrast, in the carotid artery ligation model, no effect of genetic deletion of the sEH was observed.

EETs are potent endogenous compounds with beneficial vascular actions.[7] Because the sEH limits EET availability, inhibition of this enzyme has emerged as an option for treating vascular diseases. Animal experiments, which were almost exclusively performed in rodents, suggested that sEH inhibition lowers blood pressure in some hypertensive models[9,11] and that a reduction of sEH activity has antiinflammatory effects in a variety of disease conditions.[14] Thus, we

hypothesized that sEH inhibition should strongly prevent neointima formation.

It was therefore an unexpected finding that the lack of sEH activity interfered with the neointima development only in the femoral cuff model and not in the carotid artery ligation model. The latter observation is strengthened by the recent report that the ligation-induced remodeling of the carotid artery is also sEH independent.[15] The carotid artery ligation model and the femoral artery cuff model, however, differ in their consequences on NO formation, the site of injury, and the accompanying processes in the adventitia. For example, the carotid ligation artery model, but not the femoral cuff model, is devoid of shear stress–induced NO release. Thus, in the latter model, genetic knockout of the endothelial nitric oxide synthase promoted disease progression.[4] Moreover, the femoral cuff model exhibits high inflammatory activity, as it was made evident by the induction of inducible nitric oxide synthase,[4] and increased tumor necrosis factor-α expression.[16] Accordingly, inflammatory components are of central relevance for neointima formation since direct stimulation with the toll-like receptor 4 ligand lipopolysaccharide further increased neointima formation in the femoral artery cuff model,[17] and corticosteroids attenuated it.[18]

The pathophysiology of neointima formation in response to carotid artery ligation also involves endothelial activation, inflammation, and cytokine production,[3,19,20] but the withdrawal of flow-induced production of endothelium-derived NO is considered to be the main stimulus.[21] In addition, pronounced apoptosis of SMCs occurs within the first 2 days after the intervention.[22] For other vascular injury models, it has been demonstrated that the extent of the subsequent proliferation of SMCs in the media occurs in relation to the extent of SMC apoptosis.[23] Apoptotic cells also have strong antiinflammatory properties, as they induce M2 macrophage polarization.[24] This mechanism may limit the inflammation in the carotid ligation model. Although the present study did not focus on apoptosis, it is conceivable that the pronounced antiinflammatory effects of sEH inhibitors are less effective in the carotid ligation model or that sEH inhibitors interfere with the apoptotic process.

Given that NO production is increased in the femoral cuff model, it should be mentioned that NO appears to play a major role in mediating the biological effects of EETs in the mouse.[25] EETs activate the phosphatidylinositol 3-kinase,[26] increase via AKT the activity of endothelial nitric oxide synthase, and protect endothelial cells from apoptosis. Importantly, knockout of sEH has also been shown to increase phosphatidylinositol 3-kinase activity, which protected cardiac function after ischemia.[27] Moreover, it has recently been shown that the beneficial effects of sEH inhibition are not observed in the wire-injury–induced vascular remodeling model of the femoral artery in C57BL/6 mice, which is characterized by endothelial denudation.[15]

A large number of studies have supported the hypothesis that sEH inhibition exerts beneficial vascular and antiinflammatory effects. Accordingly, in the present work, attenuated neointima formation in femoral arteries of $sEH^{-/-}$ and sEH inhibitor-treated mice was associated with reduced proliferation of cells in the media of the vessels, as well as attenuated expression of COX2, CTGF, and Gro-β. Interestingly, expression of tumor necrosis factor-α, which is derived primarily from macrophages, was unaffected by the lack of sEH. This suggests some specificity of the antiinflammatory property of EETs. It has been suggested that EETs directly interfere with the activation of nuclear factor κB[28] in the vasculature, and such a process would affect COX2 and Gro-β expression, as also observed in the present study. Both proteins could contribute to neointima formation through a chemotactic and proinflammatory effect. The control of the CTGF expression is complex and predominantly involves transforming growth factor β, hypoxia, and mechanical stress.[29] In addition to its profibrotic effects, CTGF promotes proliferation,[29] and thus attenuated CTGF expression in femoral arteries of animals which lack sEH could contribute to attenuated SMC proliferation observed in this group. Alternatively, as previously noted in cultured SMCs, sEH inhibition can attenuate the proliferation of SMCs by a direct effect on the cell cycle.[30]

The final step of neointima formation involves the migration of SMCs from the medial layer into the subintimal space. It was previously demonstrated in rat SMCs that EETs attenuate migration activity in a transwell assay.[31] Nevertheless, in the present study, a specific antimigratory effect of EETs on murine aortic vascular SMCs was not observed, as DHETs were as effective as EETs in preventing migration in cultured cells (data not shown). This suggests that in vivo complex secondary effects, potentially via the action of NO, contribute to the actions of EETs or that local concentrations in the model vary from those used in culture systems and derived from plasma level determinations. Indeed, a limitation of the present study was that EETs and DHETs were only measured in the plasma, but even with pooling samples it was not possible to obtain sufficient tissue for reliable mass spectroscopy analyses.

It has been suggested that sEH inhibitors also reduce the progression of atherosclerotic disease in $ApoE^{-/-}$ mice.[32] Although this finding might not be unexpected on the basis of our observations, it should be mentioned that the proatherosclerotic protocol used in the latter study involved the chronic infusion of angiotensin II in combination with an atherogenic diet. Angiotensin II, however, induces strong vascular inflammation,[33] and a high-fat diet aggravates the situation by inducing fatty liver inflammation.[34] Thus, the "antiatherosclerotic" action might rather be an antiinflammatory one, and additional experiments in "aged" $ApoE^{-/-}$ and $ApoE^{-/-}\times sEH^{-/-}$ mice, as well as population-based studies on the different sEH polymorphisms, will be needed to uncover the true contribution of sEH to this disease.

In conclusion, in the present study we provide evidence that the beneficial vascular effects of sEH inhibition extend beyond the pressure-lowering effect and that sEH inhibitors may be attractive therapeutics for attenuating neointima formation in some disease conditions.

Acknowledgments

The authors are grateful for the excellent technical assistance of Katalin Wandzioch, Sina Bätz, and Tanja Schönfelder. We thank Erik Maronde for his support concerning measurement of PKA activity.

Sources of Funding

This study was supported by the Deutsche Forschungsgemeinschaft, Exzellenzcluster 147 "Cardio-Pulmonary Systems," the Medical Faculty of the Goethe-University, the LOEWE Lipid Signalling Forschungszentrum Frankfurt, the National Institute of Environmental Health Sciences (grant R37 ER02710), and the NIH (grant HL59699).

Disclosures

B.D. Hammock founded Arete Therapeutics to develop sEH inhibitors and move them into clinical trials.

References

1. Schwartz SM. Perspectives series: cell adhesion in vascular biology: smooth muscle migration in atherosclerosis and restenosis. *J Clin Invest*. 1997;99:2814–2816.
2. Satoh K, Berk BC. Circulating smooth muscle progenitor cells: novel players in plaque stability. *Cardiovasc Res*. 2008;77:445–447.
3. Tang PC, Qin L, Zielonka J, Zhou J, Matte-Martone C, Bergaya S, van RN, Shlomchik WD, Min W, Sessa WC, Pober JS, Tellides G. MyD88-dependent, superoxide-initiated inflammation is necessary for flow-mediated inward remodeling of conduit arteries. *J Exp Med*. 2008;205:3159–3171.
4. Moroi M, Zhang L, Yasuda T, Virmani R, Gold HK, Fishman MC, Huang PL. Interaction of genetic deficiency of endothelial nitric oxide, gender, and pregnancy in vascular response to injury in mice. *J Clin Invest*. 1998;101:1225–1232.
5. Lardenoye JH, Delsing DJ, de Vries MR, Deckers MM, Princen HM, Havekes LM, van H, V, van Bockel JH, Quax PH. Accelerated atherosclerosis by placement of a perivascular cuff and a cholesterol-rich diet in ApoE*3Leiden transgenic mice. *Circ Res*. 2000;87:248–253.
6. Kumar A, Lindner V. Remodeling with neointima formation in the mouse carotid artery after cessation of blood flow. *Arterioscler Thromb Vasc Biol*. 1997;17:2238–2244.
7. Larsen BT, Campbell WB, Gutterman DD. Beyond vasodilatation: non-vasomotor roles of epoxyeicosatrienoic acids in the cardiovascular system. *Trends Pharmacol Sci*. 2007;28:32–38.
8. Arand M, Cronin A, Adamska M, Oesch F. Epoxide hydrolases: structure, function, mechanism, and assay. *Methods Enzymol*. 2005;400:569–588.
9. Jung O, Brandes RP, Kim IH, Schweda F, Schmidt R, Hammock BD, Busse R, Fleming I. Soluble epoxide hydrolase is a main effector of angiotensin II-induced hypertension. *Hypertension*. 2005;45:759–765.
10. Imig JD, Zhao X, Capdevila JH, Morisseau C, Hammock BD. Soluble epoxide hydrolase inhibition lowers arterial blood pressure in angiotensin II hypertension. *Hypertension*. 2002;39:690–694.
11. Sinal CJ, Miyata M, Tohkin M, Nagata K, Bend JR, Gonzalez FJ. Targeted disruption of soluble epoxide hydrolase reveals a role in blood pressure regulation. *J Biol Chem*. 2000;275:40504–40510.
12. Morisseau C, Goodrow MH, Newman JW, Wheelock CE, Dowdy DL, Hammock BD. Structural refinement of inhibitors of urea-based soluble epoxide hydrolases. *Biochem Pharmacol*. 2002;63:1599–1608.
13. Michaelis UR, Fisslthaler B, Barbosa-Sicard E, Falck JR, Fleming I, Busse R. Cytochrome P450 epoxygenases 2C8 and 2C9 are implicated in hypoxia-induced endothelial cell migration and angiogenesis. *J Cell Sci*. 2005;118:5489–5498.
14. Schmelzer KR, Kubala L, Newman JW, Kim IH, Eiserich JP, Hammock BD. Soluble epoxide hydrolase is a therapeutic target for acute inflammation. *Proc Natl Acad Sci USA*. 2005;102:9772–9777.
15. Simpkins AN, Rudic RD, Roy S, Tsai HJ, Hammock BD, Imig JD. Soluble epoxide hydrolase inhibition modulates vascular remodeling. *Am J Physiol Heart Circ Physiol.* 2010;298:H795–H806.
16. Monraats PS, Pires NM, Schepers A, Agema WR, Boesten LS, de Vries MR, Zwinderman AH, de Maat MP, Doevendans PA, de Winter RJ, Tio RA, Waltenberger J, 't Hart LM, Frants RR, Quax PH, van Vlijmen BJ, Havekes LM, van der LA, van der Wall EE, Jukema JW. Tumor necrosis factor-alpha plays an important role in restenosis development. *FASEB J*. 2005;19:1998–2004.
17. Hollestelle SC, de Vries MR, Van Keulen JK, Schoneveld AH, Vink A, Strijder CF, Van Middelaar BJ, Pasterkamp G, Quax PH, De Kleijn DP. Toll-like receptor 4 is involved in outward arterial remodeling. *Circulation*. 2004;109:393–398.
18. Pires NM, Schepers A, van der Hoeven BL, de Vries MR, Boesten LS, Jukema JW, Quax PH. Histopathologic alterations following local delivery of dexamethasone to inhibit restenosis in murine arteries. *Cardiovasc Res*. 2005;68:415–424.
19. Kumar A, Hoover JL, Simmons CA, Lindner V, Shebuski RJ. Remodeling and neointimal formation in the carotid artery of normal and P-selectin-deficient mice. *Circulation*. 1997;96:4333–4342.
20. Kawasaki T, Dewerchin M, Lijnen HR, Vreys I, Vermylen J, Hoylaerts MF. Mouse carotid artery ligation induces platelet-leukocyte-dependent luminal fibrin, required for neointima development. *Circ Res*. 2001;88:159–166.
21. Rudic RD, Shesely EG, Maeda N, Smithies O, Segal SS, Sessa WC. Direct evidence for the importance of endothelium-derived nitric oxide in vascular remodeling. *J Clin Invest*. 1998;101:731–736.
22. Cho A, Mitchell L, Koopmans D, Langille BL. Effects of changes in blood flow rate on cell death and cell proliferation in carotid arteries of immature rabbits. *Circ Res*. 1997;81:328–337.
23. Fingerle J, Au YP, Clowes AW, Reidy MA. Intimal lesion formation in rat carotid arteries after endothelial denudation in absence of medial injury. *Arteriosclerosis*. 1990;10:1082–1087.
24. Savill J, Dransfield I, Gregory C, Haslett C. A blast from the past: clearance of apoptotic cells regulates immune responses. *Nat Rev Immunol*. 2002;2:965–975.
25. Hercule HC, Schunck WH, Gross V, Seringer J, Leung FP, Weldon SM, da Costa Goncalves AC, Huang Y, Luft FC, Gollasch M. Interaction between P450 eicosanoids and nitric oxide in the control of arterial tone in mice. *Arterioscler Thromb Vasc Biol*. 2009;29:54–60.
26. Yang S, Lin L, Chen JX, Lee CR, Seubert JM, Wang Y, Wang H, Chao ZR, Tao DD, Gong JP, Lu ZY, Wang DW, Zeldin DC. Cytochrome P-450 epoxygenases protect endothelial cells from apoptosis induced by tumor necrosis factor-alpha via MAPK and PI3K/Akt signaling pathways. *Am J Physiol Heart Circ Physiol*. 2007;293:H142–H151.
27. Seubert JM, Sinal CJ, Graves J, Degraff LM, Bradbury JA, Lee CR, Goralski K, Carey MA, Luria A, Newman JW, Hammock BD, Falck JR, Roberts H, Rockman HA, Murphy E, Zeldin DC. Role of soluble epoxide hydrolase in postischemic recovery of heart contractile function. *Circ Res*. 2006;99:442–450.
28. Node K, Huo Y, Ruan X, Yang B, Spiecker M, Ley K, Zeldin DC, Liao JK. Anti-inflammatory properties of cytochrome P450 epoxygenase-derived eicosanoids. *Science*. 1999;285:1276–1279.
29. de WP, Leoni P, Abraham D. Connective tissue growth factor: structure-function relationships of a mosaic, multifunctional protein. *Growth Factors*. 2008;26:80–91.
30. Davis BB, Thompson DA, Howard LL, Morisseau C, Hammock BD, Weiss RH. Inhibitors of soluble epoxide hydrolase attenuate vascular smooth muscle cell proliferation. *Proc Natl Acad Sci USA*. 2002;99:2222–2227.
31. Sun J, Sui X, Bradbury JA, Zeldin DC, Conte MS, Liao JK. Inhibition of vascular smooth muscle cell migration by cytochrome p450 epoxygenase-derived eicosanoids. *Circ Res*. 2002;90:1020–1027.
32. Ulu A, Davis BB, Tsai HJ, Kim IH, Morisseau C, Inceoglu B, Fiehn O, Hammock BD, Weiss RH. Soluble epoxide hydrolase inhibitors reduce the development of atherosclerosis in apolipoprotein e-knockout mouse model. *J Cardiovasc Pharmacol*. 2008;52:314–323.
33. Marchesi C, Paradis P, Schiffrin EL. Role of the renin-angiotensin system in vascular inflammation. *Trends Pharmacol Sci*. 2008;29:367–374.
34. Ludwig J, McGill DB, Lindor KD. Review: nonalcoholic steatohepatitis. *J Gastroenterol Hepatol*. 1997;12:398–403.

Soluble epoxide hydrolase deficiency attenuates neo-intima formation in the femoral cuff model of hyperlipidemic mice

Marc Revermann, Manuel Schloss, Eduardo Barbosa-Sicard, Anja Mieth, Stefan Liebner, Christophe Morisseau, Gerd Geisslinger, Ralph T. Schermuly, Ingrid Fleming, Bruce D. Hammock, Ralf P. Brandes

Materials and methods: Extended Version for the online supplement

Animal treatment

The experiments were performed in accordance with the National Institutes of Health Guidelines on the Use of Laboratory Animals. Both the University Animal Care Committee and the Federal Authorities for Animal Research of the Regierungsprasidium Darmstadt (Hessen, Germany) approved the study protocol. C57/BL6-ApoE$^{-/-}$ (F10) breeding pairs (ApoE$^{-/-}$) were purchased from Charles Rivers (Deisenhofen, Germany). C57/BL6-sEH$^{-/-}$ mice (F5, sEH$^{-/-}$) were kindly supplied by F. Gonzalez (NIH, Bethesda, MD) [1], backcrossed for 5 additional generations into the C57/BL6 strain and subsequently crossed with ApoE$^{-/-}$ mice to obtain ApoE-sEH double knockout animals. ApoE$^{-/-}$ x sEH$^{-/-}$ were backcrossed more than 7 times to obtain ApoE$^{-/-}$ x sEH$^{+/+}$. For the sake of readability, ApoE$^{-/-}$ x sEH$^{+/+}$ are denominated as "ApoE$^{-/-}$". Standard chow was fed to the animals (Ssniff, Soest, Germany; 87,7% dry substance, 19% protein, 3,3% fat, 4,9% crude fiber, 6,4%crude ashe, 54,1% N-free extractives, 36,5% starch, 4,7% sugar; brutto energy 16,3 MJ/kg). Experiments were performed exclusively in male ApoE$^{-/-}$ and ApoE$^{-/-}$ sEH$^{-/-}$ mice starting at an age of 12 weeks. The sEH inhibitor 12-(3-adamantan-1-yl-ureido)-dodecanoic acid (AUDA) [2] was administered to the animals via drinking water. Preparation of the solutions was as follows: AUDA (100 mg) was dissolved in ethanol (0.05% of final solution), water and 1 per cent (of final solution) 2-hydroxypropyl-b-cyclodextrin. AUDA was encapsulated by ultrasound treatment for 10 min, and the solution was then added to normal water, yielding a final concentration of 100 mg/l.

Femoral artery cuff model

Neo-intima formation and accelerated atherosclerosis was induced by means of vascular injury through cuff placement around the femoral arteries of mice as described previously [3;4]. Briefly, femoral arteries were isolated from surrounding tissues and a non-constricting 2mm polyethylene cuff (internal diameter 0.58mm; outer diameter 0,96mm) was placed around the arteries. After this intervention, a neo-intima formation developed within 2 weeks. Animals were sacrificed 14 days after cuff placement. Tissue segments were harvested after perfusion fixation (4% para-formaldehyde in phosphate buffered saline/pH 7.4; 3min; 100mmHg) cuffs were removed and tissues were embedded in paraffin and cut in 4µm thick slices. After standard H&E staining, 5 sections equally distributed within the cuff region were analyzed by planimetry using ImageJ software (NIH). The total cross-sectional medial area was measured between the external and internal elastic lamina; the total cross-sectional intimal area was measured between the endothelial cell monolayer and the internal elastic lamina.

Vessel diameter was calculated based on perimetrical measurements applying the mathematical circumference formula. Animals which developed no measurable neo-intima were defined as non-responders and excluded from analysis.

Carotid artery ligation

The left common carotid artery was dissected and ligated near the carotid bifurcation using a silk suture (7-0) as described previously [5]. After 4 weeks, the animals were killed and the carotid arteries were excised after perfusion fixation (4% para-formaldehyde in phosphate buffered saline/pH 7.4; 3min; 100mmHg). The tissue was embedded in paraffin and cut into 4µm thick slices. After H&E staining, 5 representative sections of the medial carotid artery (5mm length) were analyzed planimetrically.

Evaluation of in-situ cell proliferation

Animals received a single intraperitoneal injection of 5-bromo-2-deoxy-uridine (BrdU - Roche Applied Science, Mannheim, Germany, /150 mg/kg body weight) dissolved in PBS (100 µl / animal) 24 h before sacrifice. BrdU was visualized using a commercially available kit (Roche) in deparaffinized artery sections with the modification that the antigens were unmasked by heating in citrate buffer (pH6.1). BrdU was

detected using an anti-BrdU primary antibody (Roche Applied Science) and visualized by an Alexa546 coupled secondary antibody (1:300, Invitrogen, Karlsruhe, Germany). α-smooth muscle actin was detected by a directly labeled fluorescein isothiocyanate (FITC)-coupled monoclonal antibody (1:200; Sigma, Deisenhofen) and nuclei were counterstained using ToPro3 iodide (1:1000, Invitrogen, Karlsruhe, Germany). Images of each slice were acquired by laser scanning microscopy (LSM 510meta; Carl Zeiss, Microimaging, Jena, Germany), and BrdU-positive vascular smooth muscle cells were counted for each animal by observers blinded to the study protocol.

Immunostaining

Mouse femoral arteries were embedded in OCT tissue-freezing medium (OCT Tissue-Tec, Miles, Elkhart, Ind.) and 10µm slices were cut using a cryostat microtome. For immuno-histochemistry, slices were air-dried and permeabilized in PBS containing 0.3% Triton-X 100. Sections were blocked with 10% normal goat serum. Monocytes / macrophages were detected using rat-anti F4/80 (1:500 in PBS; Serotec, Düsseldorf, Germany) and endothelial cells were detected using rat anti-PECAM (1:100; Serotec) and visualized using the appropriate Alexa546-coupled secondary antibody (1:300 Invitrogen).

Soluble epoxide hydrolase activity assay

Frozen carotid and femoral artery tissues were grounded in liquid nitrogen and homogenized in 5 vol. of ice-cold Tris/HCl buffer (pH 7.4, 50 mmol/l) containing sucrose (250 mmol/l), potassium chloride (150 mmol/l), ethylenediaminetetraacetic acid (EDTA; 2 mmol/l), dithiothreitol (2 mmol/l; DTT), flavin adenine dinucleotide (FAD) and flavin mononucleotide (FMN; 0.5mmol/l), and phenylmethylsulfanylfluoride (PMSF; 0.25 mmol/l). Subsequently, the samples were subjected to differential centrifugation (10 min, 1000 g; 20 min, 10 000 g); the 10.000 g supernatant representing the cytosolic fraction was used for the sEH assay. The protein content was determined by standard Bradford method and sEH activity was assayed using a previously described method [6] with minor modifications. Reactions were performed at 37 °C for 20 min in a total volume of 100 µl of potassium phosphate buffer (100 mmol/L, K_2HPO_4/KH_2PO_4, pH 7.2), containing 5 µg of protein. Reactions (37°C) were started by the addition of 14,15-EET (10 µmol/L) and were stopped by placing on ice and adding ethyl acetate. Activity was measured from the amount of 14,15-DHET formed (ng14,15-DHET/µg protein/min). Experiments were performed in the absence and presence of solvent (1 % DMSO) and sEH inhibitor ACU (10 µmol/L).

Immunoblotting

For Western blot analysis, sections of the carotid and femoral arteries were directly boiled in Laemmli buffer (50 µl); the protein content was subsequently estimated by dot-blot and Amido black staining and 20µg of the samples were separated by SDS–PAGE (8%) and transferred onto nitrocellulose membrane as described [7]. Proteins were detected using antibodies against sEH (provided by one of the coauthors) and appropriate secondary antibodies labelled with infrared dyes and visualized using the Odyssey infrared imaging system (Li-COR Biosciences, Bad Homburg, Germany) system. Densitometry was carried out using the integrated odyssey software.

Determination of EETs and DHETs by LC/MS-MS

Blood samples were collected under final anaesthesia by cardiac puncture directly before pressure perfusion. After clotting for 20 minutes at room temperature and centrifugation, the serum was removed and stored at -80°C pending analysis. At a later time point, samples were spiked with deuterated internal standards (5,6-EET-d8, 8,9-EET-d8, 11,12-EET-d8 and 14,15-EET-d8 and their respective DHETs) and extracted twice with ethyl acetate (0.5 ml). The samples for the sEH activity assay were extracted in a similar way but one-tenth of organic phase was used and spiked. After evaporation of the ethyl acetate in a vacuum block under a gentle stream of nitrogen, the residues were reconstituted with 50µl of methanol/water (1:1, v/v) and analyzed with an API 4000 triple quadrupole mass spectrometer with a Turbo V source (Applied Biosystems, Darmstadt, Germany) in the negative ion mode. Precursor-to-product ion transitions of m/z 319→141 for 5,6-EET, m/z 319→154 for 8,9-EET, m/z 319→178 for 11,12-EET, m/z 319→219 for 14,15-EET, m/z 337→145 for 5,6-DHET, m/z 337→127 for 8,9-DHET, m/z 337→167 for 11,12-DHET and m/z 337→207 for 14,15-DHET were used for the multiple reaction monitoring (MRM) with a dwell time of 50 ms. as described in detail elsewhere [8]. HPLC analysis was done under gradient conditions using a Gemini NX C18 column (150 mm L x 2 mm ID, 5 µm particle size, Phenomenex, Aschaffenburg, Germany).

PCR analysis

Vessels were harvested 7 days after carotid artery ligation and femoral artery cuff placement. Carotid artery ligation area, respectively the polyethylene cuff were immediately removed and the remaining tissues shock frozen in liquid nitrogen. The vessels were grounded and lysis buffer was added. Homogenization was carried out using tissue lyser (Qiagen, Hilden, Germany) followed by RNA extraction (Absolutely RNA Miniprep Kit, Stratagene, Texas, USA) and synthesis of cDNA using a reverse transcriptase kit (Invitrogen, Karlsruhe, Germany) using random hexamer primers. Afterwards quantitative real time PCR was performed with the aid of SYBR-green PCR kit (Thermo Scientific) and a qPCR machine (Mx3005p; Stratagene, Texas, USA). Data analysis was performed by determining the relative expression using the ΔΔCt technique and elongation factor (eEF2) as house keeping gene. Mean gene mRNA expression which was measured in ApoE$^{-/-}$ vessels was set as 100 per cent. The PCR conditions were as follows: initial denaturation 95°C, 15 minutes; 40-45 cycles of denaturation (95°C, 30 seconds), annealing (60°C, 30 seconds), and elongation (72°C, 30 seconds). The following primer combinations were used: COX2: fwd: 5'-AGACACTCAGGTAGACATGATCTACCCT-3', rev: 5'-GGCACCAGACCAAAGACTTCC-3', Gro-α, fwd 5'-TGCGAAAAGAAGTGCAGAGA-3', rev: 5'-CGAGACGAGACCAGGAGAAA-3', Gro-β fwd 5'-GCTTCCTCGGGCACTCCAGAC-3', rev 5'-TTAGCCTTGCCTTTGTTCAGTAT-3', tumor necrosis factor α (TNFα): fwd: 5'-CCCGACTACGTGCTCCTCACC-3', rev: 5'-CTCCAGCTGGAAGACTCCTCCCAG-3', connective tissue growth factor (CTGF) fwd: 5'-ACCCGACTTACCAATGACAATACC-3', rev: 5'-CCGCAGAACTTAGCCCTGTATG-3', monocytes chemoattractant protein 1 (MCP-1): fwd: 5'-CCACTCACCTGCTGCTACTCATTC-3', rev: 5'-GTCACTCCTACAGAAGTGCTTGAGG-3', eEF2 fwd: 5'-GACATCACCAAGGGTGTGCAG-3', rev: 5'-GCGGTCAGCACACTGGCATA-3'

Data and statistical analysis

All values are mean ± SEM. Statistical analysis was performed using analysis of variance (ANOVA), followed by Bonferroni-corrected Fisher's LSD test, respectively, or, wherever appropriate, using an unpaired t-test. Statistical analysis for two-grouped nonparametric distributed values was performed using Mann-Whitney test. A P-value of less than 0.05 was considered as statistically significant.

References

1. Sinal CJ, Miyata M, Tohkin M, Nagata K, Bend JR, Gonzalez FJ. Targeted disruption of soluble epoxide hydrolase reveals a role in blood pressure regulation. *J Biol Chem*. 2000;275:40504-40510.

2. Morisseau C, Goodrow MH, Newman JW, Wheelock CE, Dowdy DL, Hammock BD. Structural refinement of inhibitors of urea-based soluble epoxide hydrolases. *Biochem Pharmacol*. 2002;63:1599-1608.

3. Moroi M, Zhang L, Yasuda T, Virmani R, Gold HK, Fishman MC, Huang PL. Interaction of genetic deficiency of endothelial nitric oxide, gender, and pregnancy in vascular response to injury in mice. *J Clin Invest*. 1998;101:1225-1232.

4. Lardenoye JH, Delsing DJ, de Vries MR, Deckers MM, Princen HM, Havekes LM, van Hinsbergh VW, van Bockel JH, Quax PH. Accelerated atherosclerosis by placement of a perivascular cuff and a cholesterol-rich diet in ApoE*3Leiden transgenic mice. *Circ Res*. 2000;87:248-253.

5. Kumar A, Lindner V. Remodeling with neointima formation in the mouse carotid artery after cessation of blood flow. *Arterioscler Thromb Vasc Biol*. 1997;17:2238-2244.

6. Muller DN, Schmidt C, Barbosa-Sicard E, Wellner M, Gross V, Hercule H, Markovic M, Honeck H, Luft FC, Schunck WH. Mouse Cyp4a isoforms: enzymatic properties, gender- and strain-specific expression, and role in renal 20-hydroxyeicosatetraenoic acid formation. *Biochem J*. 2007;403:109-118.

7. Jung O, Brandes RP, Kim IH, Schweda F, Schmidt R, Hammock BD, Busse R, Fleming I. Soluble epoxide hydrolase is a main effector of angiotensin II-induced hypertension. *Hypertension*. 2005;45:759-765.

8. Michaelis UR, Fisslthaler B, Barbosa-Sicard E, Falck JR, Fleming I, Busse R. Cytochrome P450 epoxygenases 2C8 and 2C9 are implicated in hypoxia-induced endothelial cell migration and angiogenesis. *J Cell Sci*. 2005;118:5489-5498.

Legends Supplementary figure 1:

I) EET and DHET regioisomer concentration and ratio measurements in ApoE$^{-/-}$ vs. ApoE$^{-/-}$ x sEH$^{-/-}$. LC/MS-MS based quantification of all EET and DHET regioisomers. N=9-10; *p<0.05. II) EET and DHET regioisomer concentration and ratio measurements in ApoE$^{-/-}$: Solvent vs. sEH inhibitor treated animals (AUDA). LC/MS-MS based quantification of all EET and DHET regioisomers. N=9-10; *p<0.05.

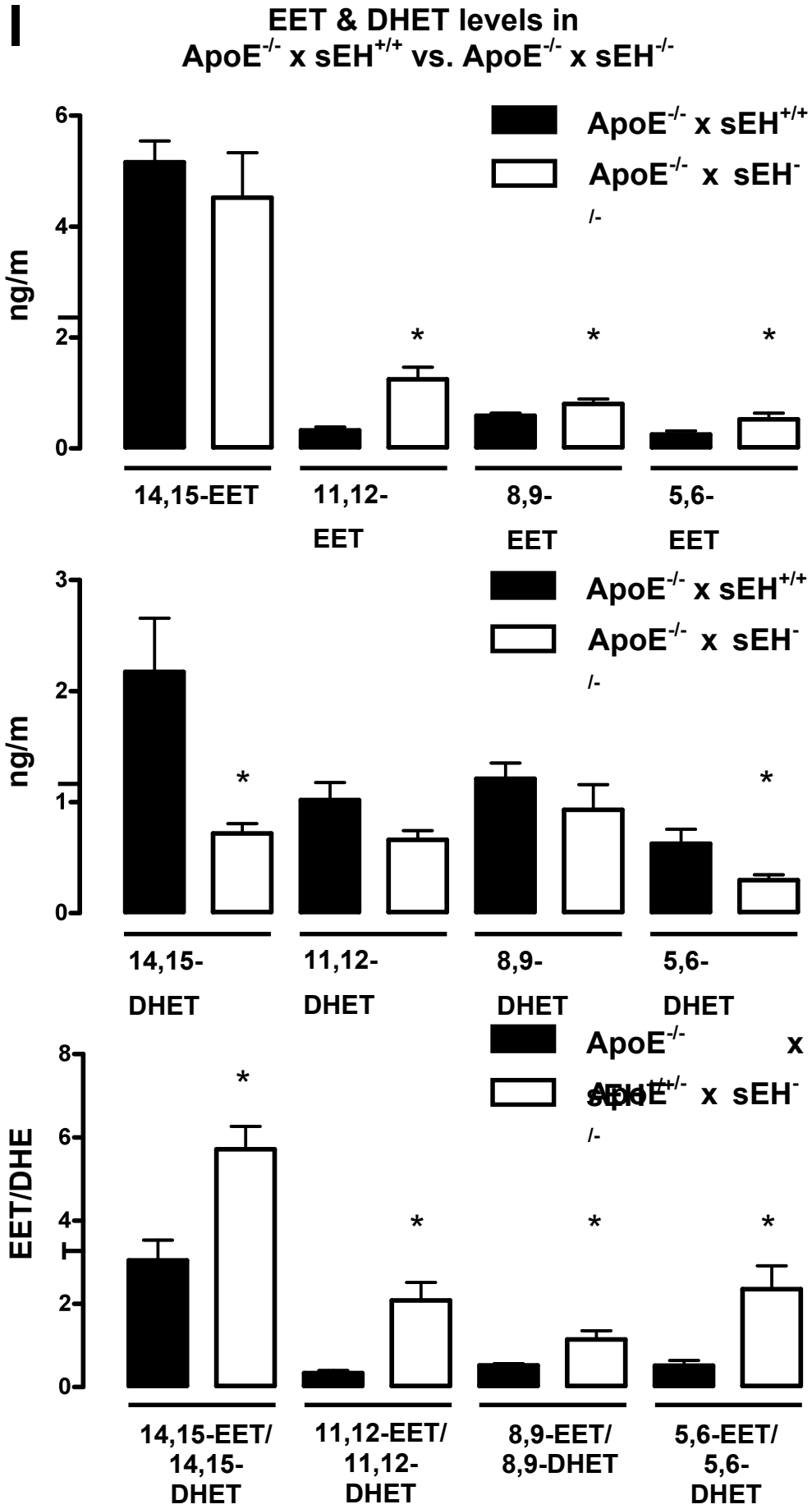

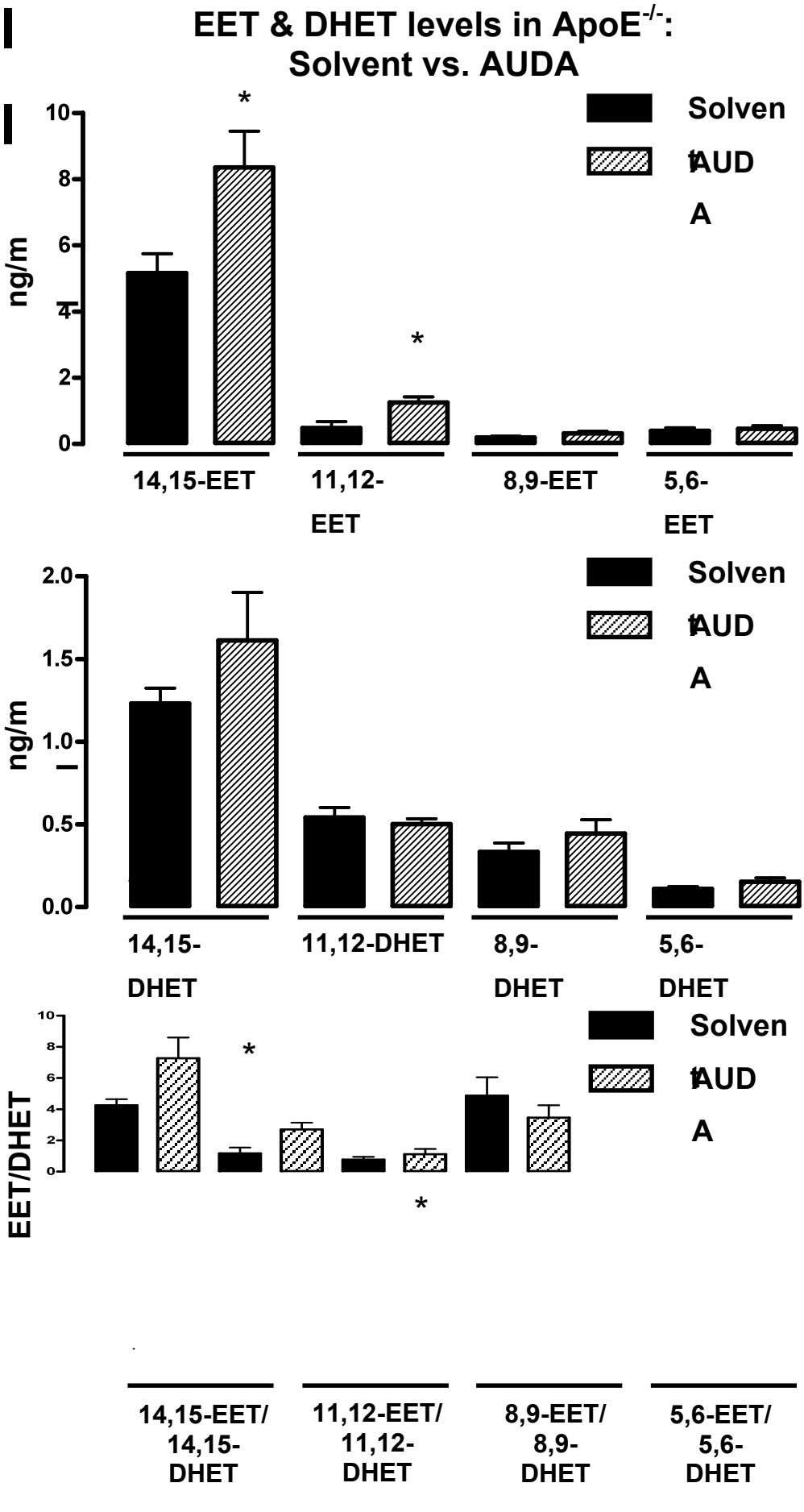

Supplement Material

I EET & DHET levels in ApoE$^{-/-}$ x sEH$^{+/+}$ vs. ApoE$^{-/-}$ x sEH$^{-/-}$

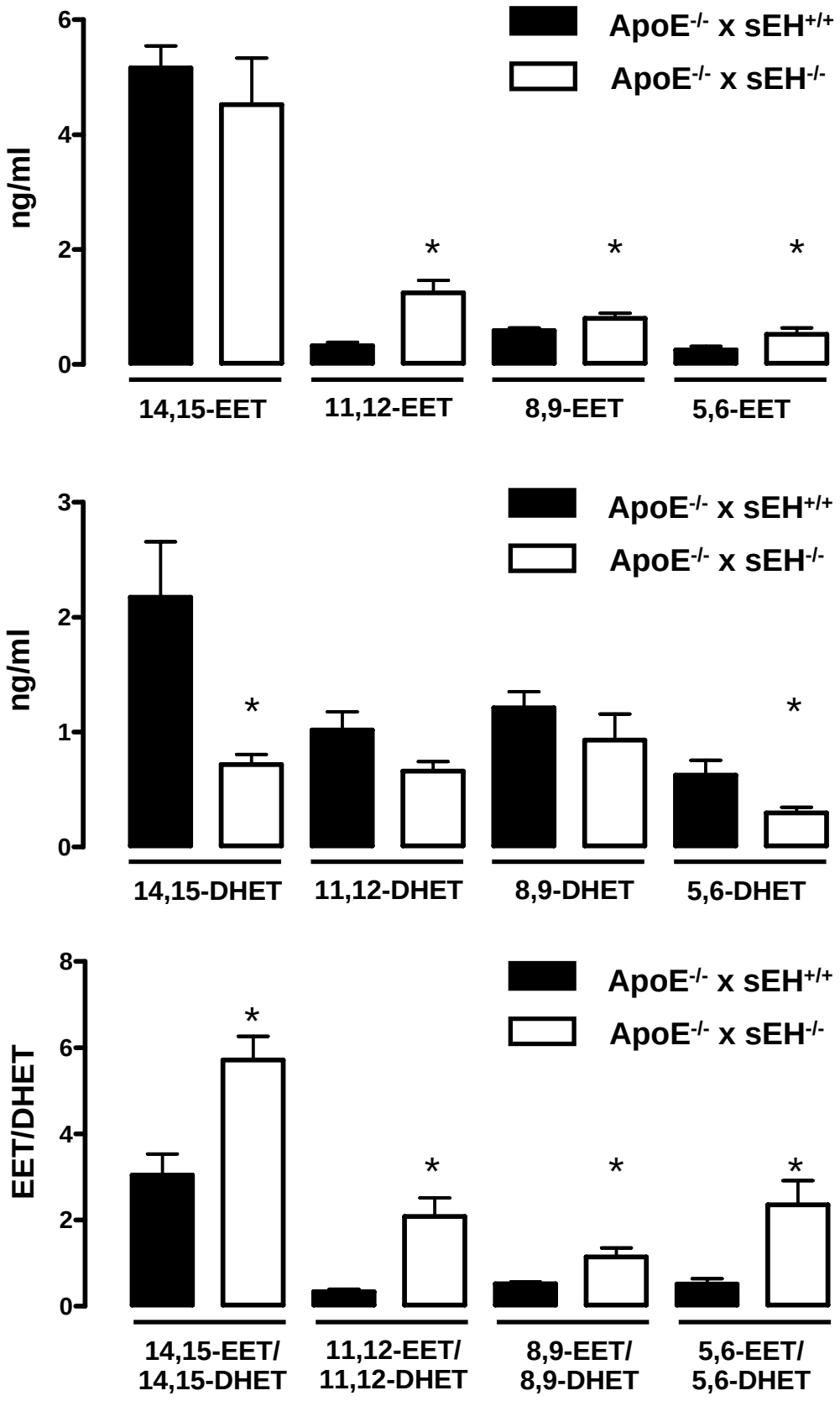

Supplement Material

II EET & DHET levels in ApoE$^{-/-}$: Solvent vs. AUDA

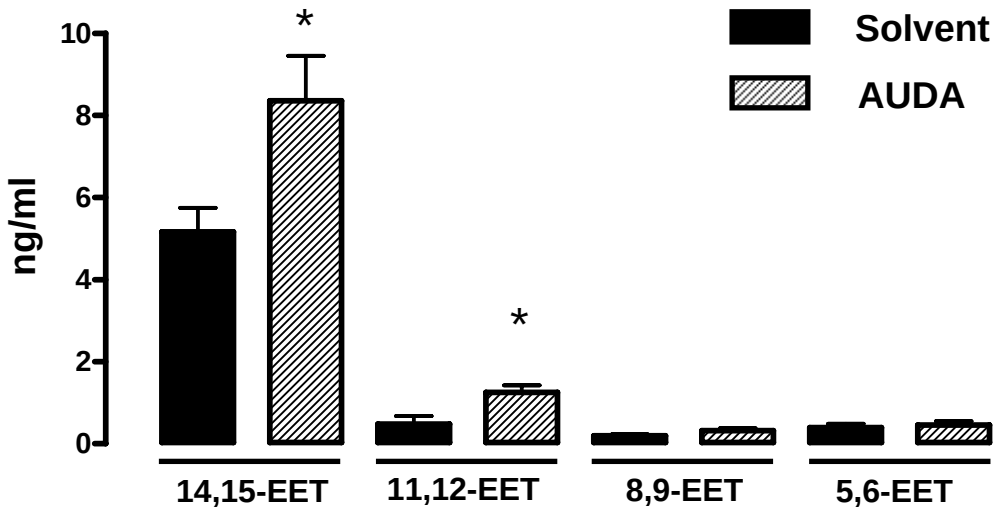

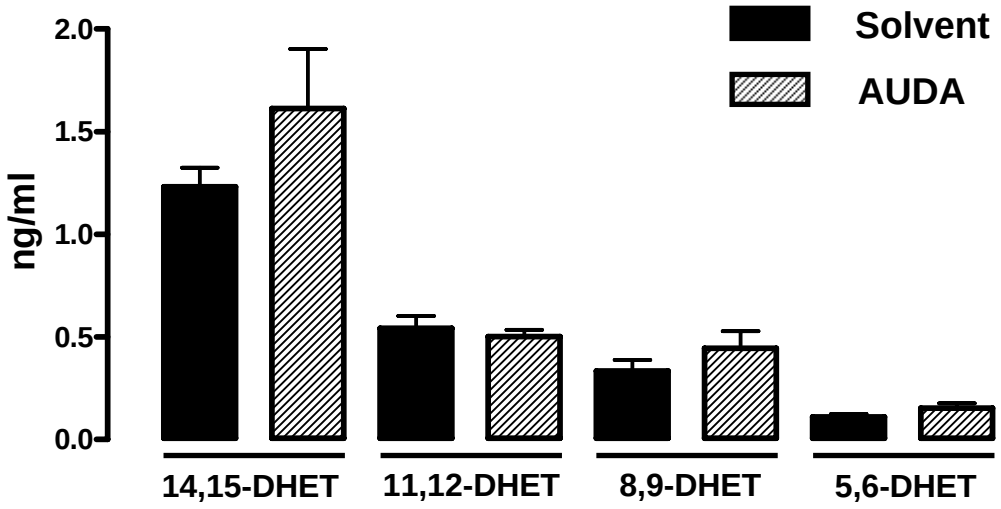

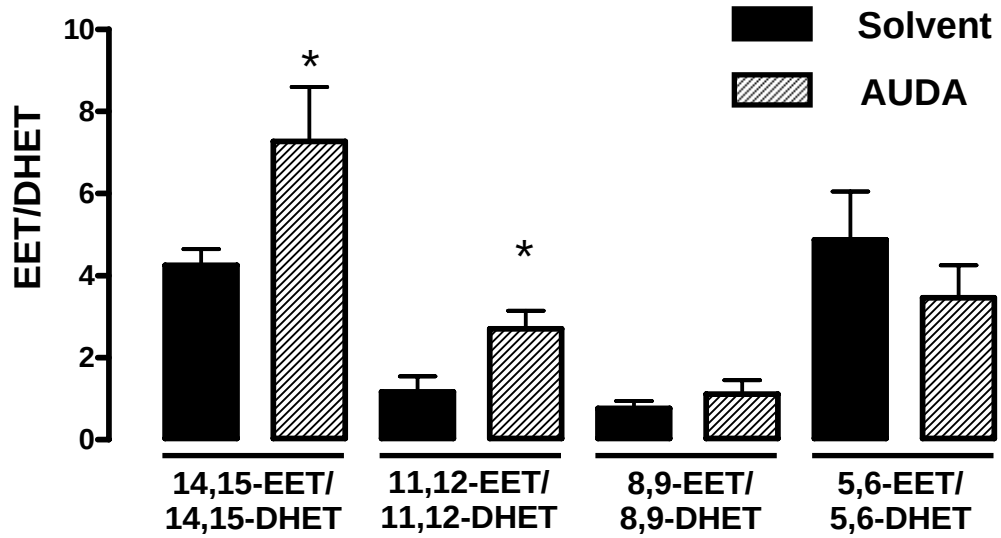

SUPPLEMENT MATERIAL

Detailed Methods

Animals

In Amsterdam, male Wistar rats (Harlan) weighing 324±9 g were kept at a constant temperature of 21±0.6°C, on a 12-h light/dark cycle and allowed free access to standard laboratory rat chow and water.

In Hobart, male hooded Wistar rats weighing 245±13 g were reared in the University of Tasmania animal house (Hobart, Australia) and allowed free access to standard laboratory rat chow (21.4% protein, 4.6% lipid, 68% carbohydrate and 6% crude fibre with added vitamins and minerals) and water *ad libitum*. All animals were housed at a constant temperature of 21±1°C, kept on a 12-h light/dark cycle.

These experiments were performed in accordance with the guidelines of the Institutional Animal Care and Use Committee of the VU University Medical Center and the University of Tasmania Animal Ethics Committee.

Isolated resistance arteries

Vasoreactivity studies were performed on resistance arteries (diameter ~100 microns) isolated from the cremaster muscle of male Wistar rats as described[1]. Effects of AICAR on muscle resistance arteries were studied ex vivo by exposing cremaster resistance arteries to the AMPK agonist AICAR (0.2 and 2 mM; n=4 and n=7, respectively). The acute effects of AICAR

on vascular tone following exposure of the arteries to AICAR were monitored for 30 min. To assess whether AICAR's vasoactive effects were mediated by the vascular endothelium, effects of AICAR (2 mM) were studied after endothelium removal (n=7). Endothelium was removed by air bubble treatment as described [Eringa AJP Heart 2002]. To examine the role of NO in AICAR-induced vasodilatation, arteries were exposed to AICAR in the presence of the inhibitor of NO synthase inhibitor N-Nitro-L-arginine (n=5; L-NA, 0.1 mM; Sigma-Aldrich, St. Louis, MO). To confirm that the effects of AICAR on vascular diameter were mediated by AMPK, vasoreactivity to AICAR was studied in the presence of Compound C (40 μM; n=5), a selective inhibitor of AMPK[2]. Compound C was kindly provided by Dr Zhou of Merck Research Laboratories (Department of Molecular Endocrinology; Rahway, New Jersey). The effects of AMPK activation on endothelium-dependent vasodilatation was studied by testing responses to acetylcholine in the absence and presence of AICAR (n=3). To test whether AICAR affects smooth muscle sensitivity to NO, endothelium-denuded resistance arteries were exposed to the NO donor S-nitroso-N-acetyl penicillamine (SNAP) in the presence and absence of AICAR (n=4 per group). When >1 resistance artery segments were isolated from the same muscle, they were assigned to different experimental groups.

Enzyme activation and phosphorylation

For the determination of AICAR-mediated activation of AMPK in resistance arteries, two segments of the same resistance artery (~4 mm long , n=4 rats) were treated with either solvent or AICAR (2 mM, 30 minutes). Subsequently, the resistance artery proteins were separated by sodium dodecyl sulfate-polyacrylamide gel electrophoresis on 8% gels, transferred to a nitrocellulose membrane, and incubated with a primary antibody against Thr^{172}p-AMPKα

(1:1000; Cell Signaling Technology). After washing and addition of the secondary antibody (DAKO), protein bands were visualized using ECL reagent (Amersham Biosciences). To control for protein loading, blots were stained for ERK1 (antibody dilution 1:1000; Cell Signaling Technology).

For the determination of AICAR-mediated activation of eNOS in resistance arteries and the role of AMPK therein, cremaster resistance artery segments (~3 mm long) were treated with either solvent (n=8), AICAR (n=8; 2 mM, 30 minutes) or AICAR and compound C (n=4). Subsequently, the resistance artery proteins were separated by sodium dodecyl sulfate-polyacrylamide gel electrophoresis on 6% gels, transferred to a nitrocellulose membrane, and incubated with a primary antibody against Ser^{1177} p-eNOS (1:200; Santa Cruz). Blots were then stripped and re-probed for total eNOS (antibody: Santa Cruz; 1:200).

Densitometry of immunoblots was performed using AIDA software (Raytest, Straubenhardt, Germany), and untreated vessel samples (control) set at 1 and compared to treated vessels samples from the same animals.

Three-dimensional microscopy of Thr^{172}pAMPKα in the vessel wall

Wistar rats were anesthetized with pentobarbital sodium (70 mg/kg ip). Similar-sized, first-order cremaster resistance artery segments were dissected free, and three segments (1.5–2 mm in length, 0.1 mm inner diameter) were cut from each vessel. Muscle resistance arteries were dissected at 4°C in MOPS buffer.

Both ends of the segments were tied around glass cannulas (outer diameter ~0.1 mm) in a pressure myograph. Throughout the protocol, the transmural pressure was maintained at 65

mmHg, and flow through the vessel was zero. Segments were equilibrated at their in vivo length for 45 min before the start of the experimental protocols. Of the three resistance artery segments isolated from each rat, one was stimulated with AICAR and the other two were not stimulated. Of these two control segments, one segment was used as a negative control during microscopy (see below). At the end of the experiment, the vessels were perfusion fixed for 30 min at a pressure of 65 mm Hg with ice-cold 2% formaldehyde (in MOPS) and subsequently perfused with Triton X-100 (0.1% in MOPS) for 60 seconds to permeabilize the cells in the vessel wall. The vessel wall was stained for 1 h with anti-Thr^{172}pAMPKα (1:100, Cell Signaling Technology) and then washed again with MOPS. The fixation and staining were done at room temperature.

To visualize the stained endothelial and smooth muscle cells, the vessels were cut open longitudinally and mounted in Vectashield containing 4,6-diamidino-2-phenylindole (DAPI) on a glass coverslip with the endothelial side facing upward. Endothelium and smooth muscle were discerned by cell orientation and by nuclear morphology as described (Eringa et al. ATVB 2006). In each experiment, a negative control segment was stained without the primary antibody.

Images of the vessel wall were obtained using a ZEISS Axiovert 200 Marianas inverted microscope, equipped with a motorized stage (stepper-motor z-axis increments: 0.1 μm). A cooled CCD camera (1280 x 1024 pixels; Cooke Sensicam, Cooke, Tonawanda, NY) recorded images with true 16-bit capability. The camera is linear over its full dynamic range (up to intensities of over 4,000), whereas dark-background currents (estimated by the intensity outside the cells) are typically <100. Exposures, objective, montage, and pixel binning were automatically recorded with each image stored in memory. The microscope, camera, data viewing/processing were conducted/controlled by Slidebook software (Intelligent Imaging

Innovations, Denver, CO). Images were taken with a custom x40 air and x63 oil lens (Zeiss). The data acquisition protocol included confocal optical planes to obtain three-dimensional definition, followed by a constrained iterative deconvolution operation of the images.

Surgery for in vivo studies

All experiments were conducted using the anesthetized rat model as described previously[3-5]. Briefly, rats were anesthetized using sodium pentobarbital (50 $mg.kg^{-1}$ body weight i.p.). A tracheostomy tube was inserted to facilitate spontaneous respiration during the experiment. A carotid artery and both jugular veins were cannulated using polyethylene cannulas. The carotid artery cannula was attached to a pressure transducer (Transpac IV, Abbott Critical Systems, Morgan Hill, CA USA) allowing continuous blood pressure measurements and was also used for arterial sampling throughout the experiment. This surgical procedure lasted approximately 15 min, after which the animals were maintained under anesthesia for the remaining surgery and the duration of the experiment with a constant infusion of anesthetic (0.6 $mg.min^{-1}.kg^{-1}$ pentobarbitone sodium) via the left jugular vein. The body temperature of the animal was maintained at 37°C using a water-jacketed platform and a heating lamp positioned above the rat.

A small incision was made in the skin overlaying the femoral vessel of each hindleg. The femoral artery was carefully separated from the femoral vein and saphenous nerve and an ultrasonic flow probe (Transonic Systems, VB series 0.5nm, Ithaca, NY, USA) was placed around the femoral artery of one leg distal to the rectus abdominal muscle. The flow probe was interfaced through a flow meter to an IBM compatible computer where arterial femoral blood flow, blood pressure and heart rate were continuously measured during the experiment using

WINDAQ data acquisition software (DATAQ Instruments, Akron, OH, USA). Surgery was followed by a 60 min equilibration period to allow femoral blood flow and blood pressure to stabilize.

Two experimental groups were studied; saline and AICAR as outlined in the protocol shown in Supplementary Fig. I. AICAR infusion involved an initial bolus of 20 mg/kg followed by constant infusion of 3.75 $mg.min^{-1}.kg^{-1}$ i.v. Blood glucose concentrations were determined at the times indicated in Supplementary Fig. I. Duplicate arterial and a femoral venous blood sample (250μL) were taken at the end of the experiment. Perchloric acid extracts of plasma were analyzed for AICAR by HPLC. At the conclusion of the experiment, the gastrocnemius group of muscles of the lower leg were removed and assayed for AICAR and ZMP content. Hindleg glucose uptake was calculated by the arterial minus the venous blood glucose measurement x femoral arterial blood flow.

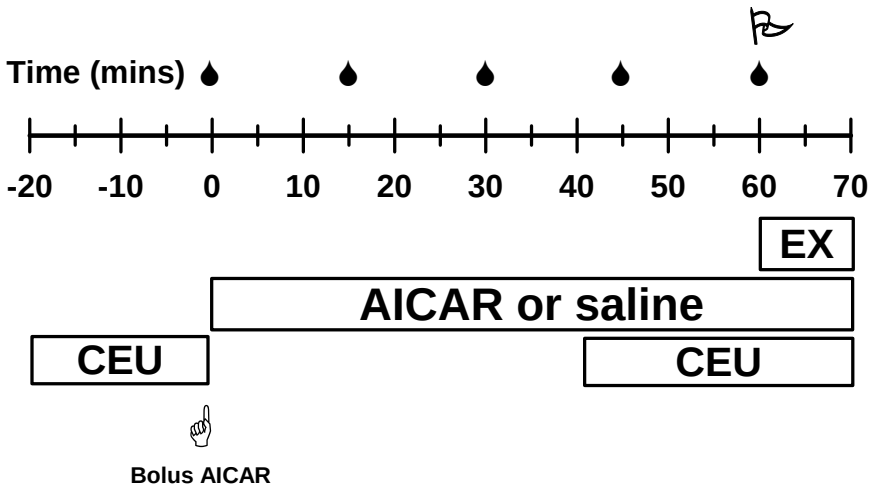

Supplementary Figure I: ***In vivo*** **Study Design.**

Either saline or AICAR was infused followed by a period of muscle contraction (EX). Arterial samples were taken for AICAR and glucose determination (♦) and venous blood samples taken for hindleg glucose uptake determination (☜). A bolus injection i.v. of AICAR (20 mg/kg) is indicated by the hand and AICAR infusion (3.75 $mg.min^{-1}.kg^{-1}$) is indicated by the bar. Microbubble infusion (40μL/min) and periods where ultrasound measurement of microvascular volume and flow rate were made are shown by contrast-enhanced ultrasound (CEU). Muscle contraction (EX) (field stimulation, 2Hz, 0.1 msec, 35V) is indicated by the box. Gastrocnemius muscle was sampled at 70 min for the determination of AICAR and ZMP content.

Contraction studies in vivo

Measurement of total blood flow by Transonic flow probes are disrupted by microbubbles. Therefore the protocol of Supplementary Fig. I was used and was in either of two formats: 1,

where a Transonic flow probe was used to measure femoral arterial blood flow; or 2, where flow probes were omitted and contrast enhanced ultrasound/microbubbles was used to measure microvascular volume and flow. Electrode wires were placed above the knee and around the Achilles tendon. Field stimulation was conducted using 0.1ms pulses at 2Hz with the voltage set at 35.

Microvascular perfusion in vivo

Details were essentially as described by Dawson et al.[5] with minor modifications. The adductor magnus and semimembranosus muscles of the hindlimb were imaged in short axis with a linear-array transducer connected to an ultrasound system (L7–4 transducer, HDI-5000, ATL Ultrasound). Pulse inversion imaging was performed at a centerline transmission frequency of 3.3 MHz. The mechanical index [(peak acoustic pressure)×(frequency)$^{-1/2}$], a measure of acoustic power, was set at 0.8 to destroy and image microbubbles with the same pulse[6]. The acoustic focus was placed at the mid-muscle level and gain settings were optimized and held constant throughout the experiment. Albumin microbubbles (Optison, GE Healthcare) were infused via the jugular vein at 40μL/min for the duration of data acquisition. Intermittent imaging was performed using pulsing intervals (PI) from 0.5 to 15s to allow incremental microvascular (capillary) replenishment with microbubbles between each pulse until the volume within the beam was completely refilled[7]. Several frames were acquired at each PI. Data were transferred to an offline computer and analyzed using QLAB^{TM} software (Version 2.0, Philips Ultrasound, Bothwell, USA). The ultrasound intensity in decibels within the region of interest (semimembranosus, adductor magnus, and biceps femoris muscles) were converted to acoustic intensity and after background subtraction using 0.5s ultrasound images (thus removing signals

from the large rapid flow vessels), a pulsing interval (time) versus acoustic-intensity curve was plotted. This allowed calculation of microvascular volume (A) as well as microvascular flow rate (A x β) according to the equation $y=A\ (1-e^{-\beta(t-0.5)})$ where y is the acoustic intensity at a given pulsing interval[8].

Statistics

Steady-state responses are reported as mean changes in diameter from baseline (in percent)±standard error (SE). The baseline diameter was defined as the arterial diameter just before addition of AICAR. Diameter responses to AICAR and L-NA were tested using a one sample t test against a theoretical value of zero. Differences between groups were analyzed using one-way ANOVA and Bonferroni post hoc tests. Differences in pAMPK and p-eNOS staining were tested with Student's t-tests. Effects of AICAR on measures made *in vivo* (blood pressure, heart rate, femoral blood flow and contrast-enhanced ultrasound measures) were statistically analysed by two-way repeated measures analysis of variance and Student-Newman-Keuls post hoc tests. Differences were considered statistically significant when $P<0.05$.

References

1. Eringa EC, Stehouwer CD, Merlijn T, Westerhof N, Sipkema P. Physiological concentrations of insulin induce endothelin-mediated vasoconstriction during inhibition of NOS or PI3-kinase in skeletal muscle arterioles. *Cardiovasc Res*. 2002;56:464-471.

2. Zhou G, Myers R, Li Y, Chen Y, Shen X, Fenyk-Melody J, Wu M, Ventre J, Doebber T, Fujii N, Musi N, Hirshman MF, Goodyear LJ, Moller DE. Role of AMP-activated protein kinase in mechanism of metformin action. *J Clin Invest*. 2001;108:1167-1174.

3. Rattigan S, Clark MG, Barrett EJ. Hemodynamic actions of insulin in rat skeletal muscle: evidence for capillary recruitment. *Diabetes*. 1997;46:1381-1388.

4. Rattigan S, Clark MG, Barrett EJ. Acute vasoconstriction-induced insulin resistance in rat muscle in vivo. *Diabetes*. 1999;48:564-569.

5. Dawson D, Vincent MA, Barrett EJ, Kaul S, Clark A, Leong-Poi H, Lindner JR. Vascular recruitment in skeletal muscle during exercise and hyperinsulinemia assessed by contrast ultrasound. *Am J Physiol Endocrinol Metab*. 2002;282:E714-E720.

6. Wei K, Jayaweera AR, Firoozan S, Linka A, Skyba DM, Kaul S. Quantification of myocardial blood flow with ultrasound-induced destruction of microbubbles administered as a constant venous infusion. *Circulation*. 1998;97:473-483.

7. Lindner JR, Wei K. Contrast echocardiography. *Curr Probl Cardiol*. 2002;27:454-519.

8. Wei K, Le E, Bin JP, Coggins M, Thorpe J, Kaul S. Quantification of renal blood flow with contrast-enhanced ultrasound. *J Am Coll Cardiol*. 2001;37:1135-1140.